Contents

Contents **1**

1 Introduction **1**

2 Temperature cycle **1**

3 Field integrals **3**
3.1 Vertical field integrals . . . 3
3.2 Horizontal field integrals . . . 4

4 Measured fields, angles, trajectories and phase errors **6**
4.1 Gap 7.2 mm . . . 6
4.2 Gap 8.0 mm . . . 6
4.3 Gap 10 mm . . . 6
4.4 Gap 15 mm . . . 6
4.5 Gap 20 mm . . . 6
4.6 Gap 25 mm . . . 7
4.7 Gap 50, 100 and 180 mm . . . 20

5 Repeatability of the effective field **23**

1 Introduction

The measurements were carried out on September 28, 2015, before realignment of the undulator. The Kugler Hall probe bench and the flip coil measured in the same positions as before the heating cycle.

2 Temperature cycle

The temperaturs during the temperature variation cycle were monitored by 6 temperature sensors. Figure 1 shows the location of the temperature sensors. Figure 2 shows the measured temperatures during the temperature variation cycle.

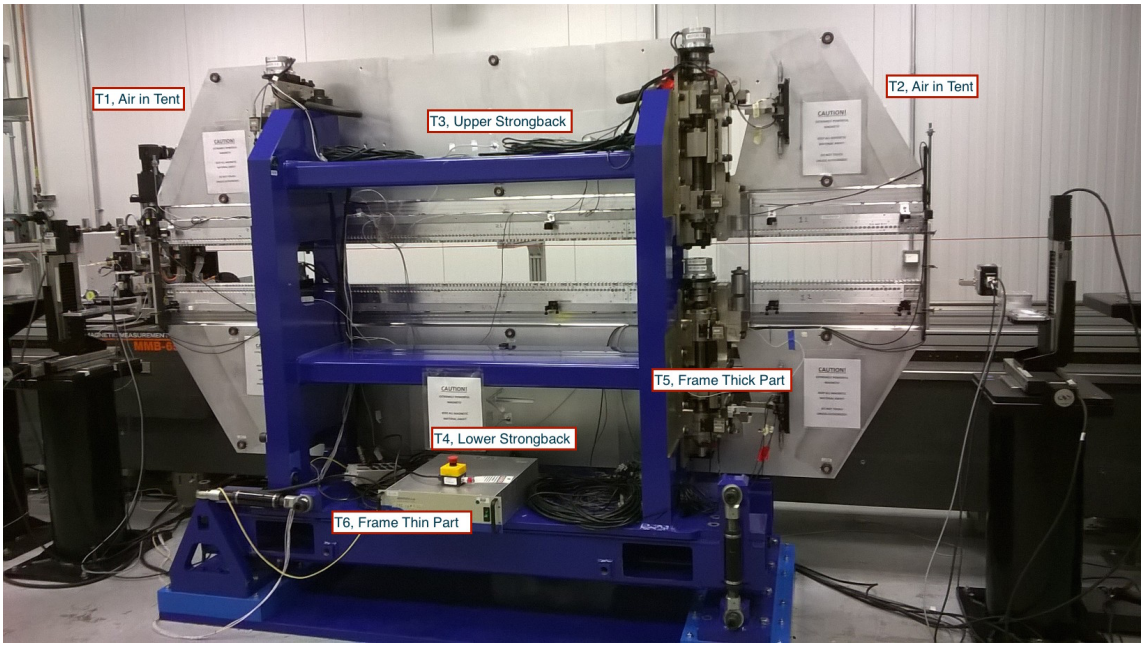

Figure 1: Location of the temperature sensors.

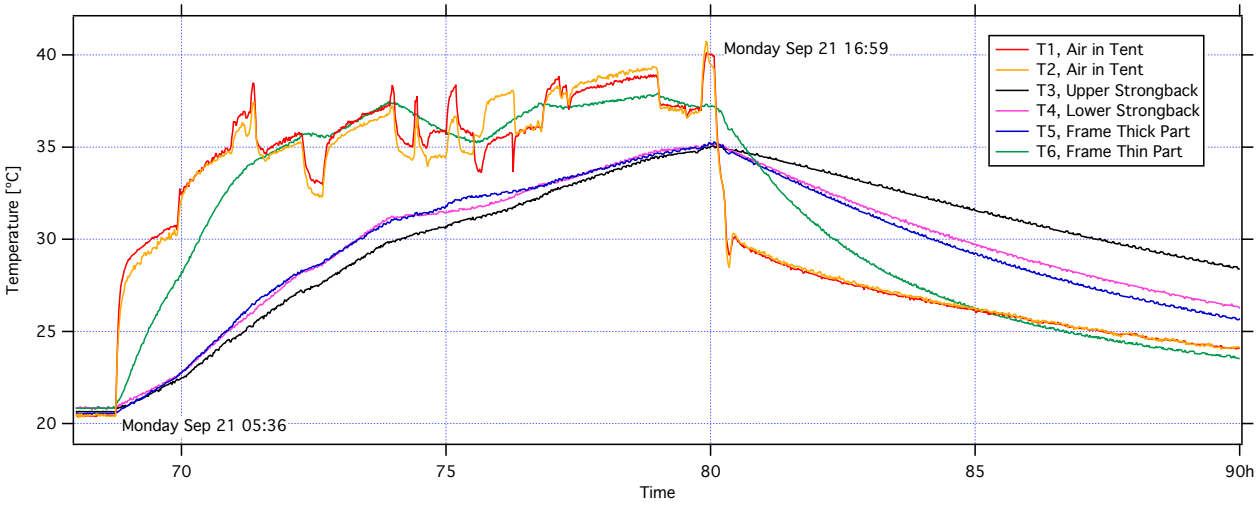

Figure 2: Measured temperature variation during the temperature cycle.

3 Field integrals

The field integrals are measured with a 3.735 m long flip coil. The diameter of the flip coil is approximately 4 mm. The vertical and horizontal field integrals have been measured on the vertical axis out from the horizontal center of the undulator in 2 mm steps out to ±20 mm horizontal deviation from the undulator axis. The multipoles up to octupole order have been found by fitting a cubic polynomial over the five central points over ±4 mm horizontal deviation from the undulator axis.

3.1 Vertical field integrals

Figure 3 shows the measured vertical field integrals at 9 different gaps. Table 1 gives the multipoles calculated from the measured field integrals by using a cubic polynomila over the 5 central points over the horizontal range ±4 mm out from the undulator axis. The background vertical field integral in UMF measured without an undulator installed is -125 Gcm.

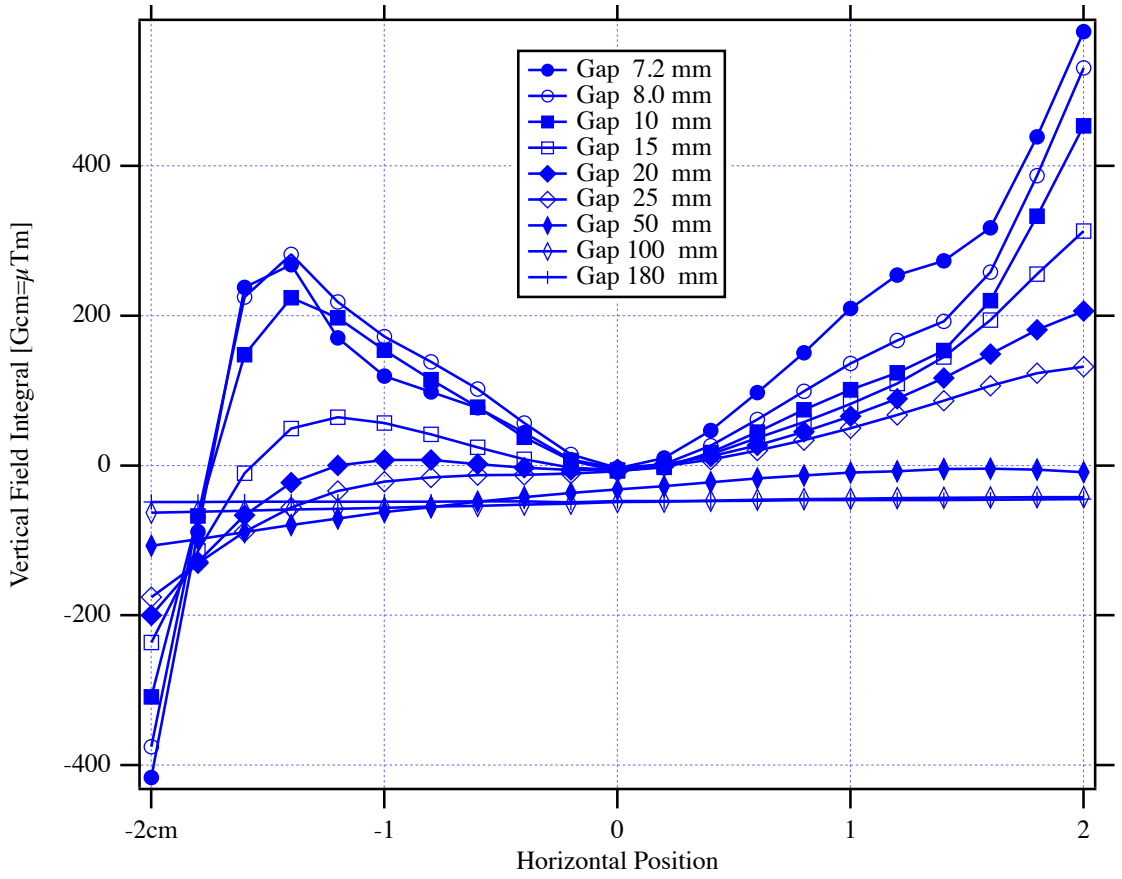

Figure 3: Vertical field integrals measured with a 3.735 m long flip coil.

3.2 Horizontal field integrals

Figure 4 shows the measured horizontal field integrals at 9 different gaps. Table 2 gives the skew multipoles calculated from the measured field integrals by using a cubic polynomila over the 5 central points over the horizontal range ±4 mm out from the undulator axis. The background horizontal field integral in UMF measured without an undulator installed is 47 Gcm.

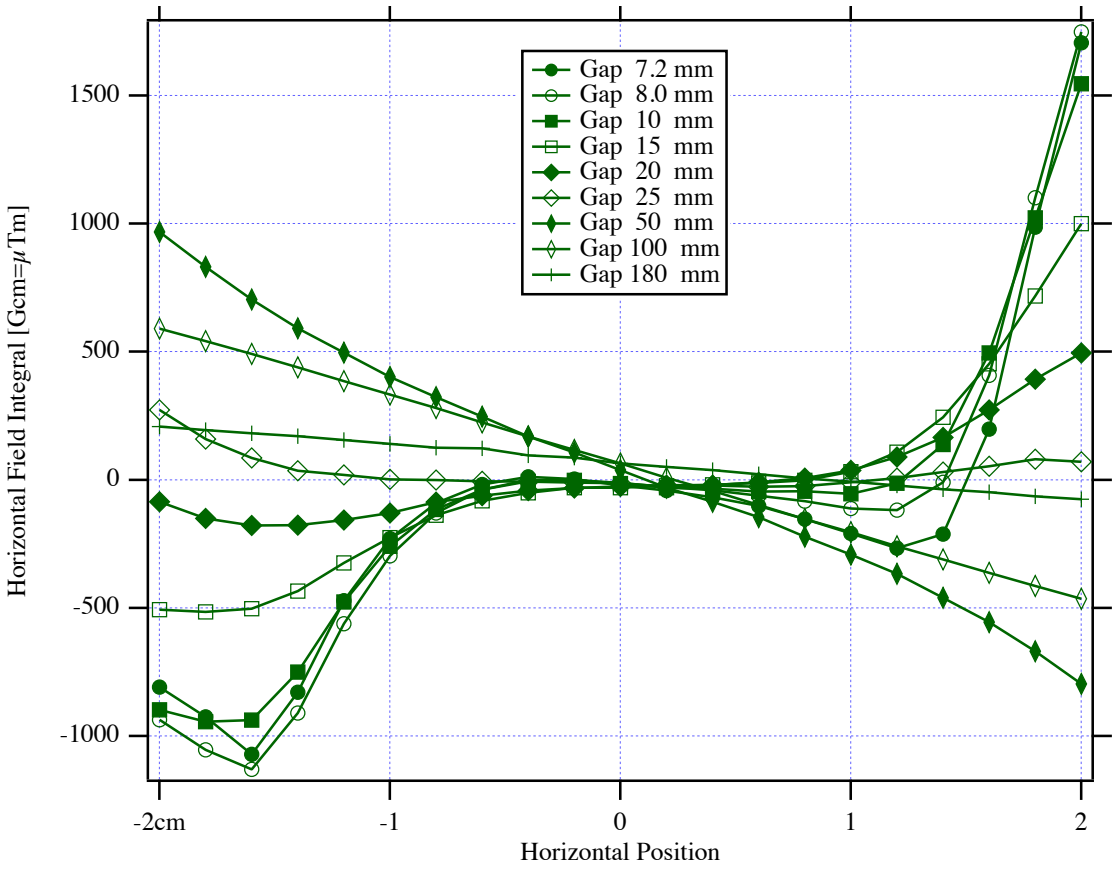

Figure 4: Horizontal field integrals measured with a 3.735 m long flip coil.

Table 1: Normal, i.e. vertical, multipoles.

Gap mm	Dipole Gcm	Quadrupole G	Sextupole G/cm	Octupole G/cm^2
7.2	-3 ±0.3	6 ±1.8	304 ±2.6	-15 ±12.8
8	-3 ±0.3	-31 ±2.1	281 ±2.9	-43 ±14.4
10	-7 ±0.4	-22 ±2.7	216 ±3.8	-19 ±18.5
15	-6 ±0.1	8 ±0.4	110 ±0.6	4 ±3
20	-5 ±0.1	19 ±1	59 ±1.4	3 ±6.9
25	-7 ±0.2	25 ±1.4	31 ±2	4 ±9.7
50	-32 ±0.2	23 ±1.3	-1 ±1.8	15 ±9
100	-49 ±0.3	6 ±2.3	-4 ±3.2	4 ±15.7
180	-48 ±0.6	6 ±4.3	2 ±6.1	-31 ±30

Table 2: Skew, i.e. horizontal, multipoles.

Gap mm	Dipole Gcm	Quadrupole G	Sextupole G/cm	Octupole G/cm^2
7.2	-19 ±2.9	-117 ±19.6	-53 ±27.6	106 ±136.1
8	-12 ±0.4	-75 ±3	-52 ±4.2	161 ±20.5
10	-14 ±0.8	-82 ±5.3	-37 ±7.5	286 ±36.8
15	-27 ±3.3	15 ±22.8	-43 ±32.1	145 ±158.2
20	-25 ±0.5	28 ±3.6	-36 ±5.1	-12 ±24.9
25	-17 ±3.1	-46 ±20.9	9 ±29.4	170 ±144.8
50	37 ±0.8	-353 ±5.5	33 ±7.7	217 ±37.9
100	64 ±0.8	-275 ±5.2	-4 ±7.4	61 ±36.3
180	67 ±2.5	-96 ±17.4	1 ±24.4	149 ±120.4

4 Measured fields, angles, trajectories and phase errors

The magnetic fields have been measured on the undulator axis in 4400 mm long Hall probe scans. The field integral found with the flip coil is used for normalizing the magetic fields measured with the Hall probe system. The normalization is done by adding or subratcing a constant field over the magnetic structure of the undulator. The constant that is added corresponds to the difference between the flip coil and the Hall probe data over the length of the flip coil.

The Hall probe scans have been carried out at 9 different gaps; 7.2, 8.0, 10, 15, 20, 25, 50, 100, and 180 mm. The magnetic fields have been analyzed for the gap range 7.2-25 mm. In the analysis the function of the aoutocorrection system for the beam position in the accelerator has been simulated by using virtual coils in the beginning and end of the 4.4 m long scan to correct the orbit of the beam passing through the undulator.

4.1 Gap 7.2 mm

The measured fields, angles, trajectories and phase errors for the HXU-32 at 7.2 mm gap is shown in Figure 5 and Figure 6, which shows the same analysis with the beam path corrected by virtual coils in the beginning and end of the scan.

4.2 Gap 8.0 mm

The measured fields, angles, trajectories and phase errors for the HXU-32 at 8.0 mm gap is shown in Figure 7 and Figure 8, which shows the same analysis with the beam path corrected by virtual coils in the beginning and end of the scan.

4.3 Gap 10 mm

The measured fields, angles, trajectories and phase errors for the HXU-32 at 10 mm gap is shown in Figure 9 and Figure 10, which shows the same analysis with the beam path corrected by virtual coils in the beginning and end of the scan.

4.4 Gap 15 mm

The measured fields, angles, trajectories and phase errors for the HXU-32 at 15 mm gap is shown in Figure 11 and Figure 12, which shows the same analysis with the beam path corrected by virtual coils in the beginning and end of the scan.

4.5 Gap 20 mm

The measured fields, angles, trajectories and phase errors for the HXU-32 at 20 mm gap is shown in Figure 13 and Figure 14, which shows the same analysis with the beam path corrected by virtual coils in the beginning and end of the scan.

4.6 Gap 25 mm

The measured fields, angles, trajectories and phase errors for the HXU-32 at 25 mm gap is shown in Figure 15 and Figure 16, which shows the same analysis with the beam path corrected by virtual coils in the beginning and end of the scan.

HXU-32
Period: 32 mm
Gap: 7.2 mm
Beff: 1.2856 T
20150928-After-Heating
Without correction coils
1st Int Ix : -11.2 [μTm]
1st Int Iy : -25.05 [μTm]
2nd Int Jx : 2.42 [μTm^2]
2nd Int Jy : 48.19 [μTm^2]
Beam energy: 4 GeV

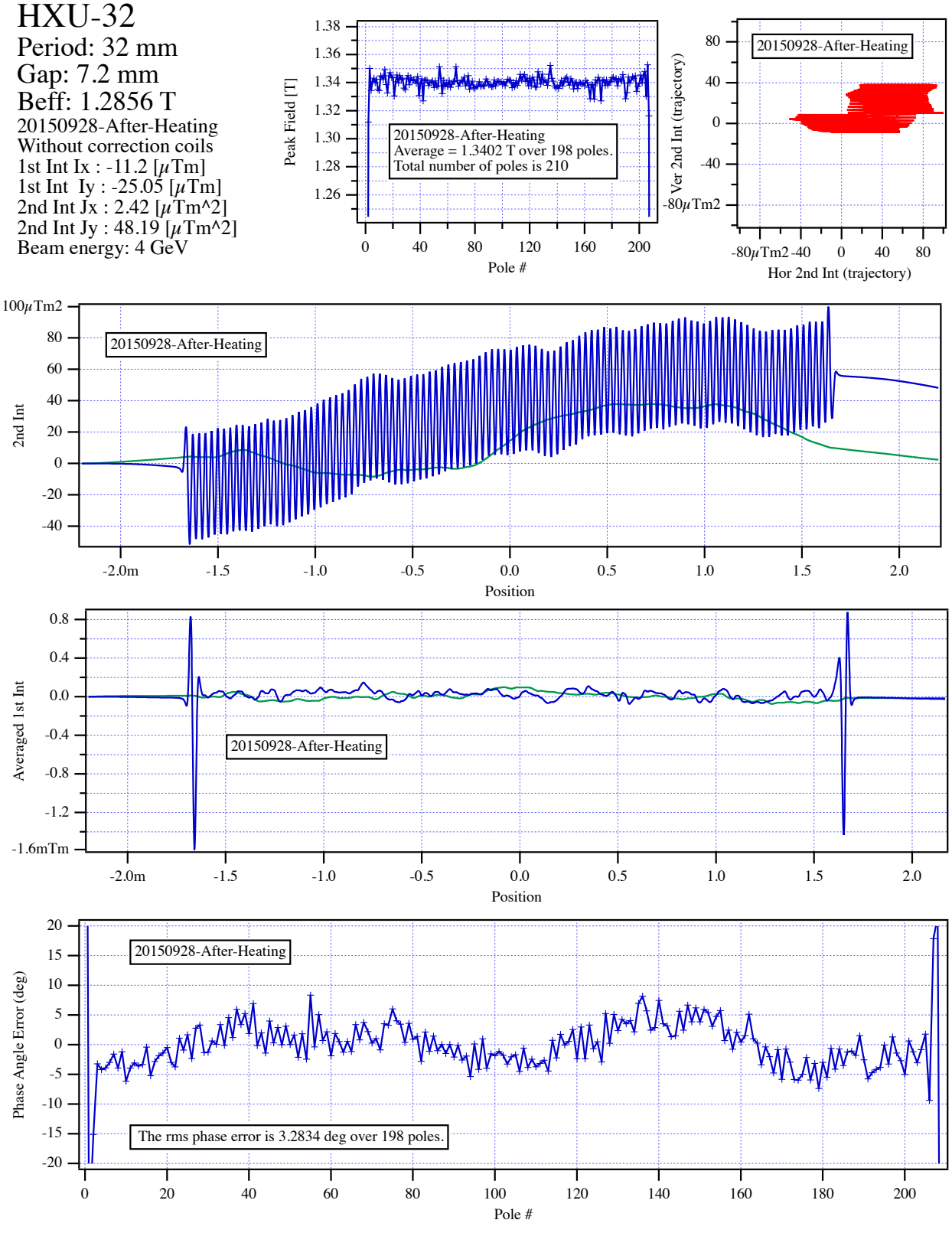

Figure 5: The measured fields, angles, trajectories and phase errors for the HXU-32 at 7.2 mm gap.

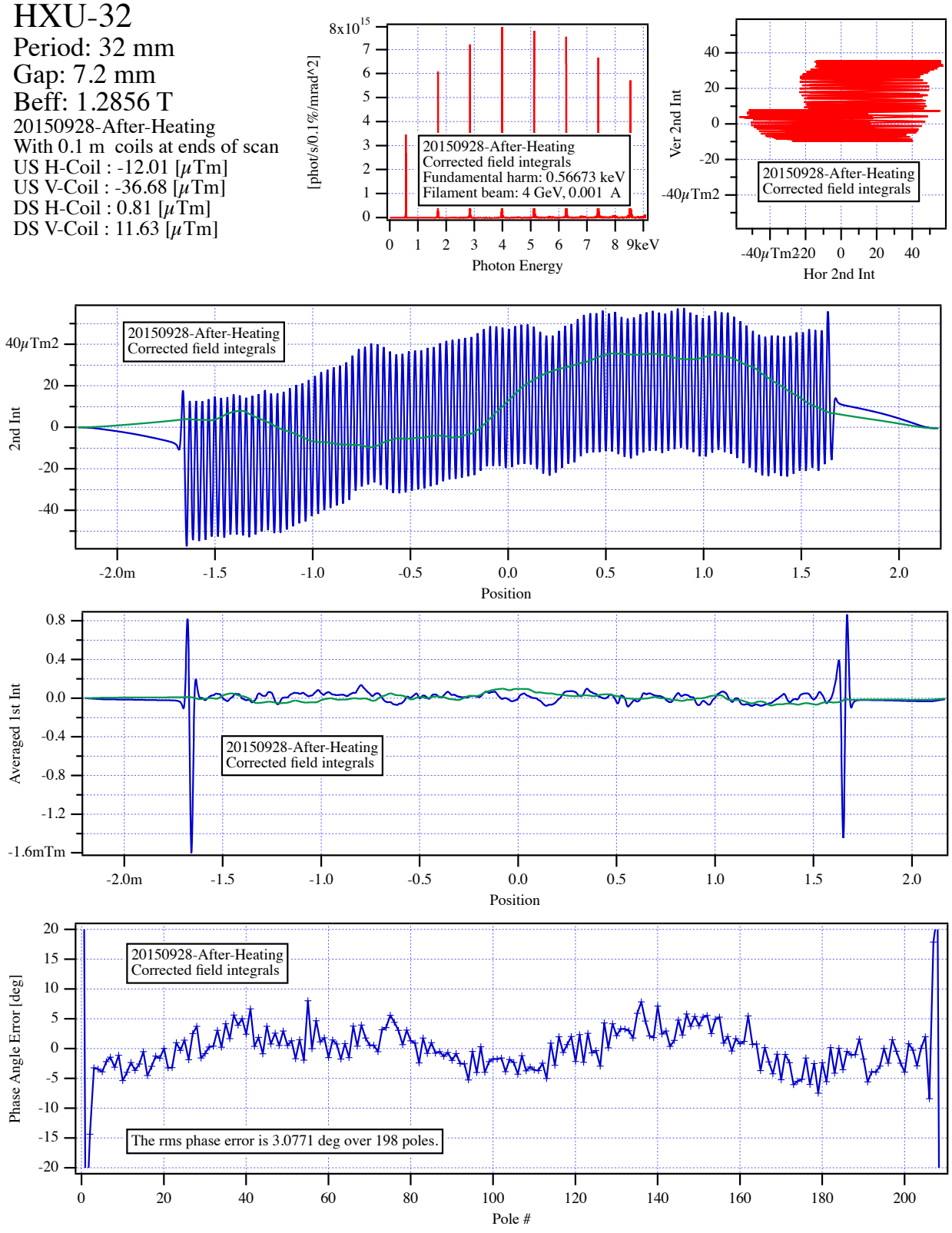

Figure 6: The measured fields, angles, trajectories and phase errors for the HXU-32 at 7.2 mm gap with the beam path corrected by virtual coils.

HXU-32
Period: 32 mm
Gap: 8 mm
Beff: 1.1611 T
20150928-After-Heating
Without correction coils
1st Int Ix : -0.23 [μTm]
1st Int Iy : -24.94 [μTm]
2nd Int Jx : 40.42 [μTm^2]
2nd Int Jy : -38.13 [μTm^2]
Beam energy: 4 GeV

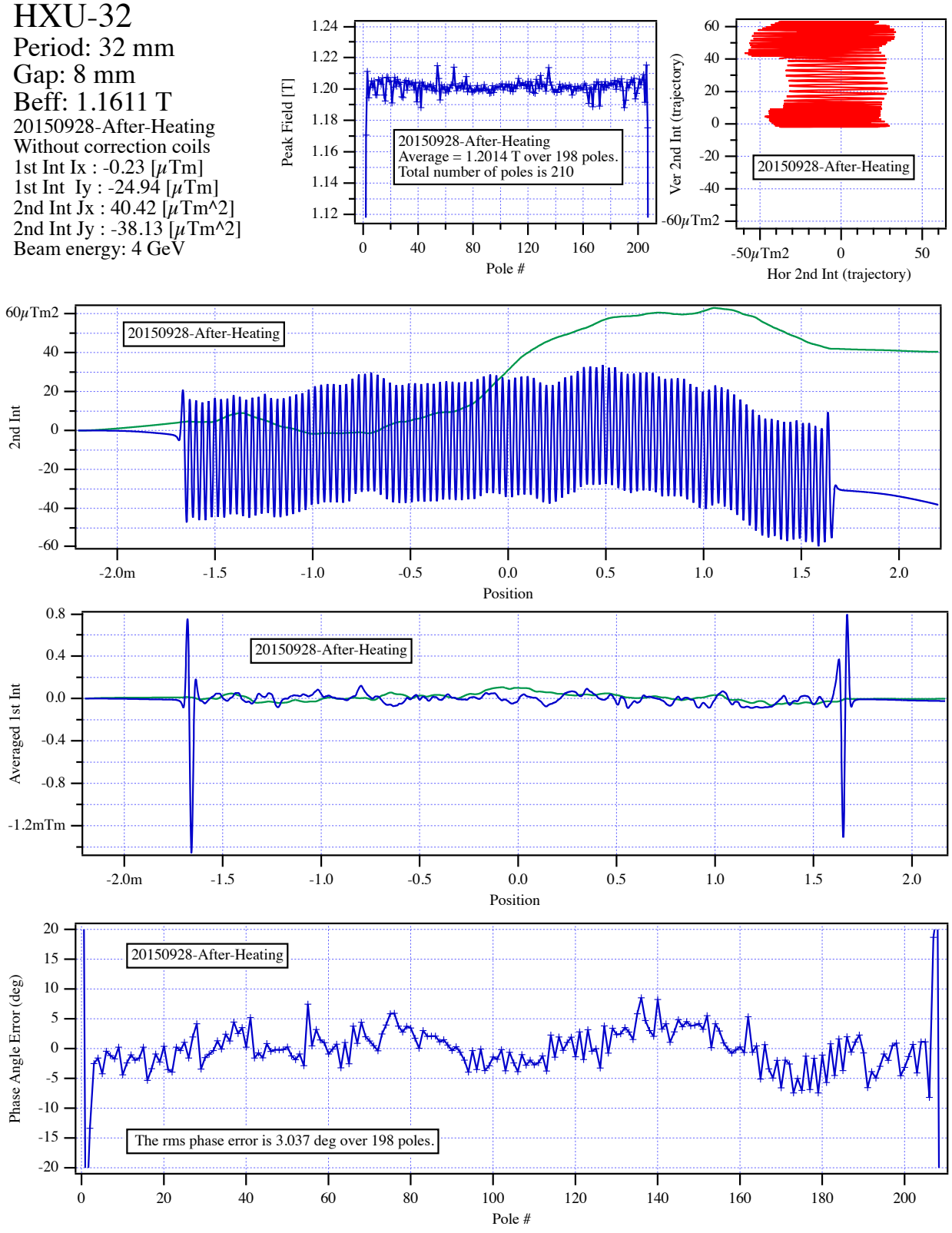

Figure 7: The measured fields, angles, trajectories and phase errors for the HXU-32 at 8.0 mm gap.

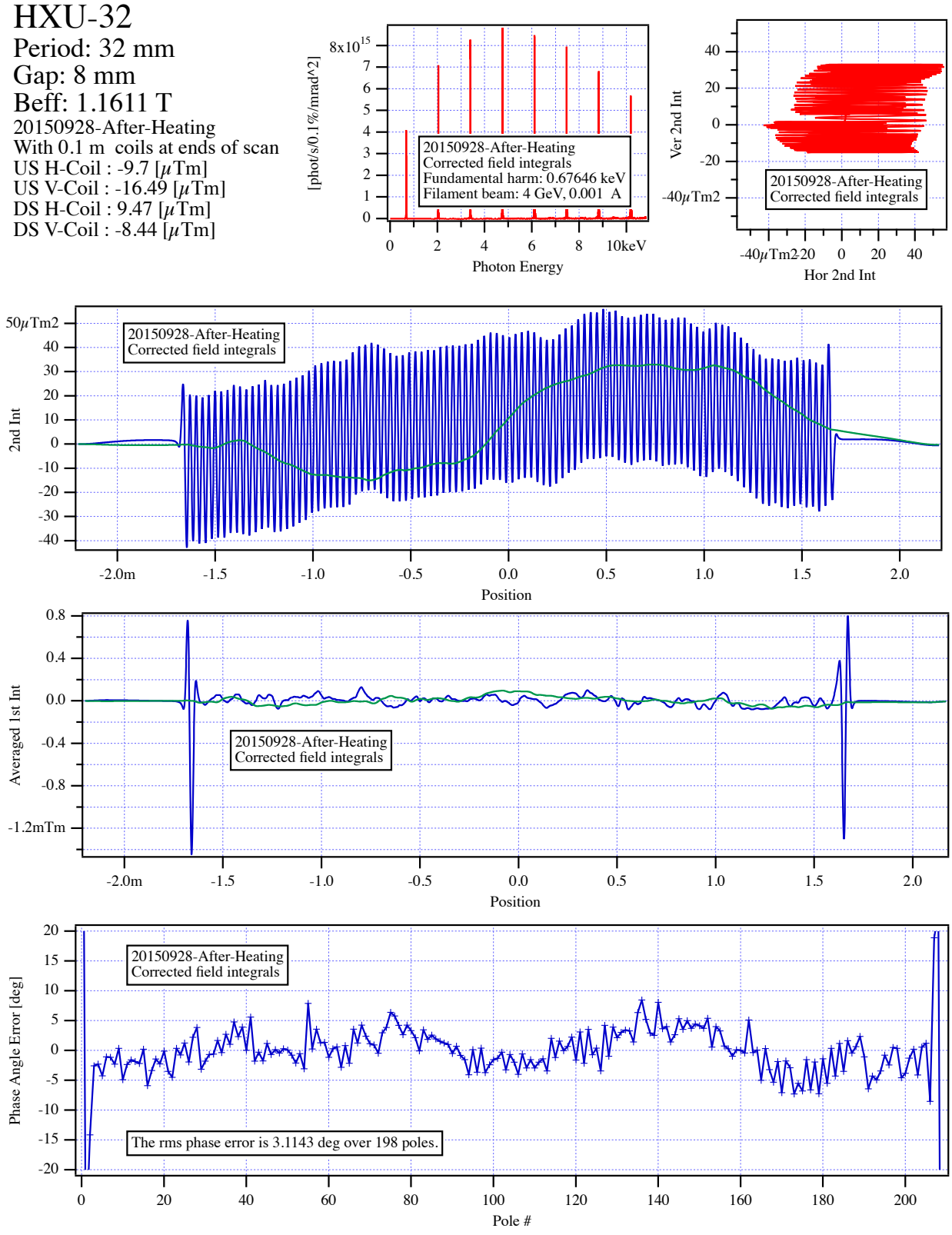

Figure 8: The measured fields, angles, trajectories and phase errors for the HXU-32 at 8.0 mm gap with the beam path corrected by virtual coils.

HXU-32
Period: 32 mm
Gap: 10 mm
Beff: 0.9057 T
20150928-After-Heating
Without correction coils
1st Int Ix : -2.86 [μTm]
1st Int Iy : -28.8 [μTm]
2nd Int Jx : 29.33 [μTm^2]
2nd Int Jy : -41.11 [μTm^2]
Beam energy: 4 GeV

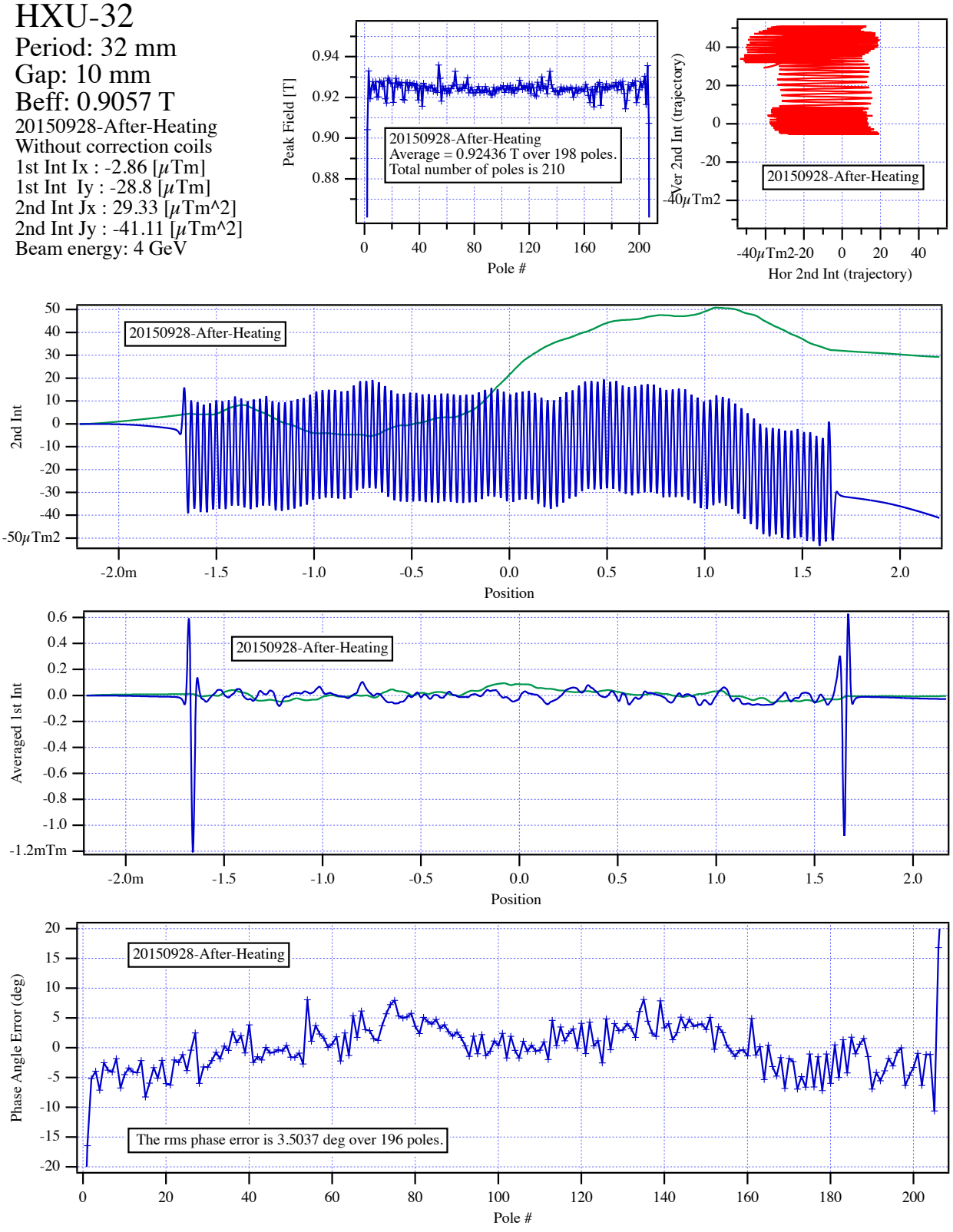

Figure 9: The measured fields, angles, trajectories and phase errors for the HXU-32 at 10 mm gap.

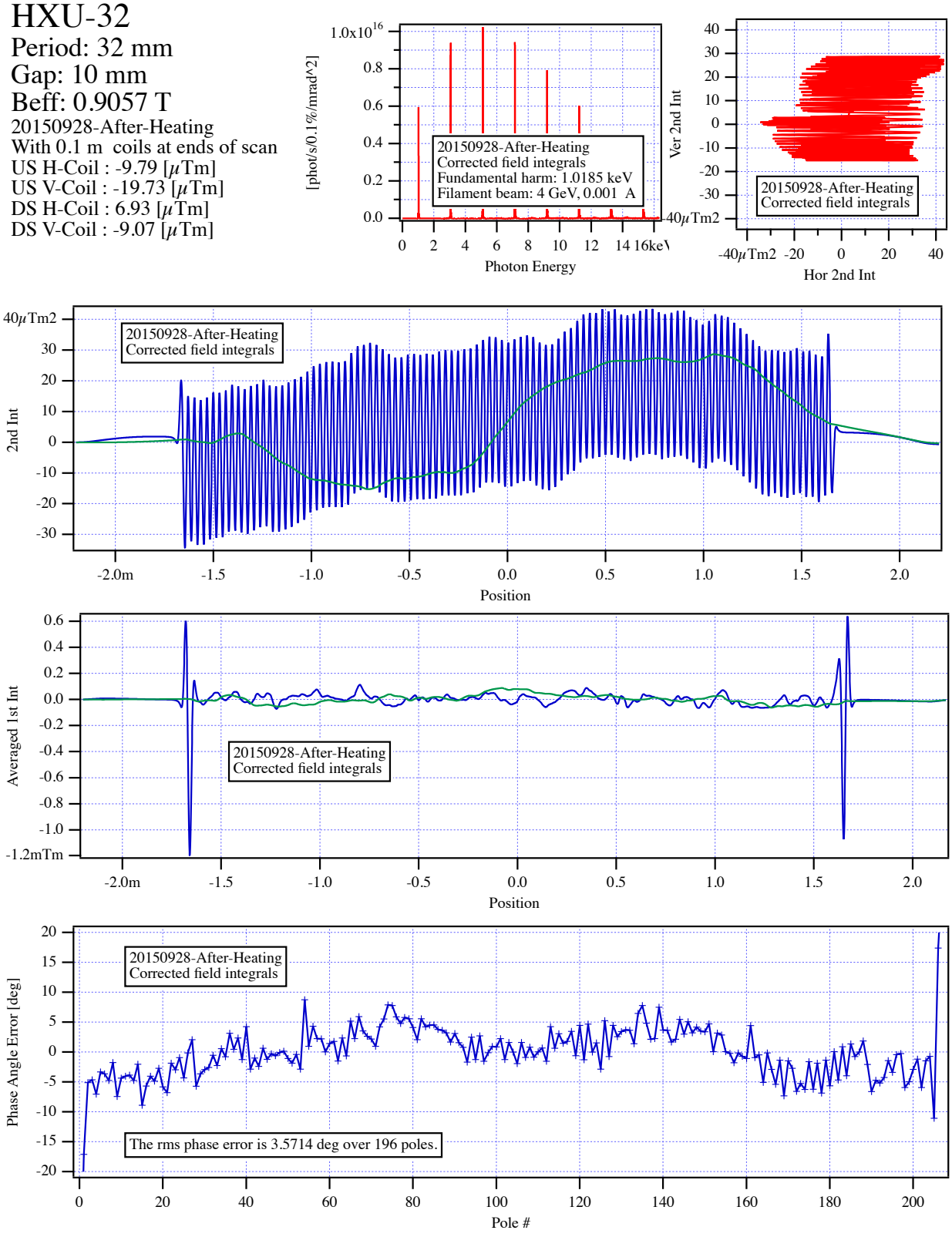

Figure 10: The measured fields, angles, trajectories and phase errors for the HXU-32 at 10 mm gap with the beam path corrected by virtual coils.

HXU-32
Period: 32 mm
Gap: 15 mm
Beff: 0.51863 T
20150928-After-Heating
Without correction coils
1st Int Ix : -19.86 [μTm]
1st Int Iy : -26.31 [μTm]
2nd Int Jx : -20.07 [μTm^2]
2nd Int Jy : -29.7 [μTm^2]
Beam energy: 4 GeV

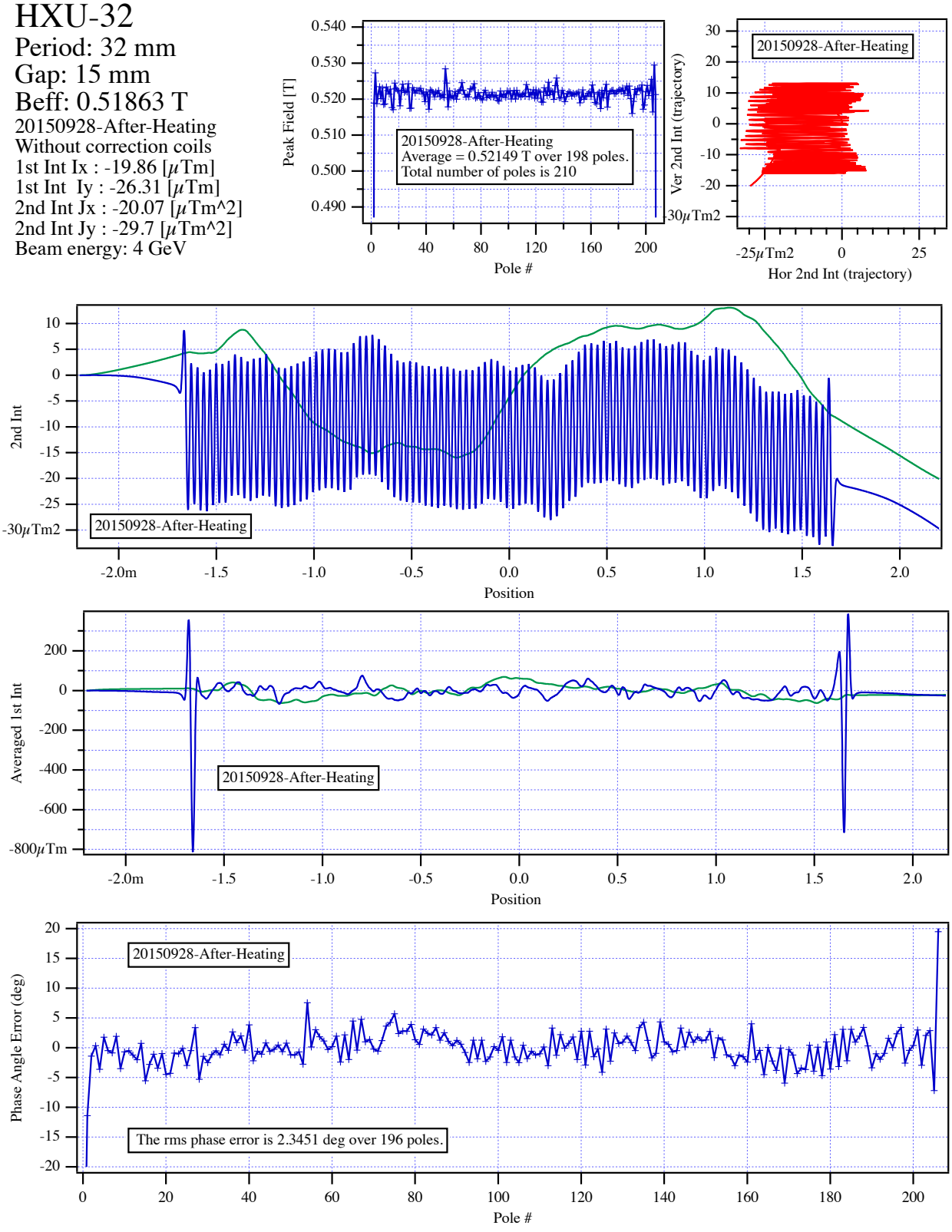

Figure 11: The measured fields, angles, trajectories and phase errors for the HXU-32 at 15 mm gap.

HXU-32
Period: 32 mm
Gap: 15 mm
Beff: 0.51863 T
20150928-After-Heating
With 0.1 m coils at ends of scan
US H-Coil : -15.6 [μTm]
US V-Coil : -19.85 [μTm]
DS H-Coil : -4.27 [μTm]
DS V-Coil : -6.46 [μTm]

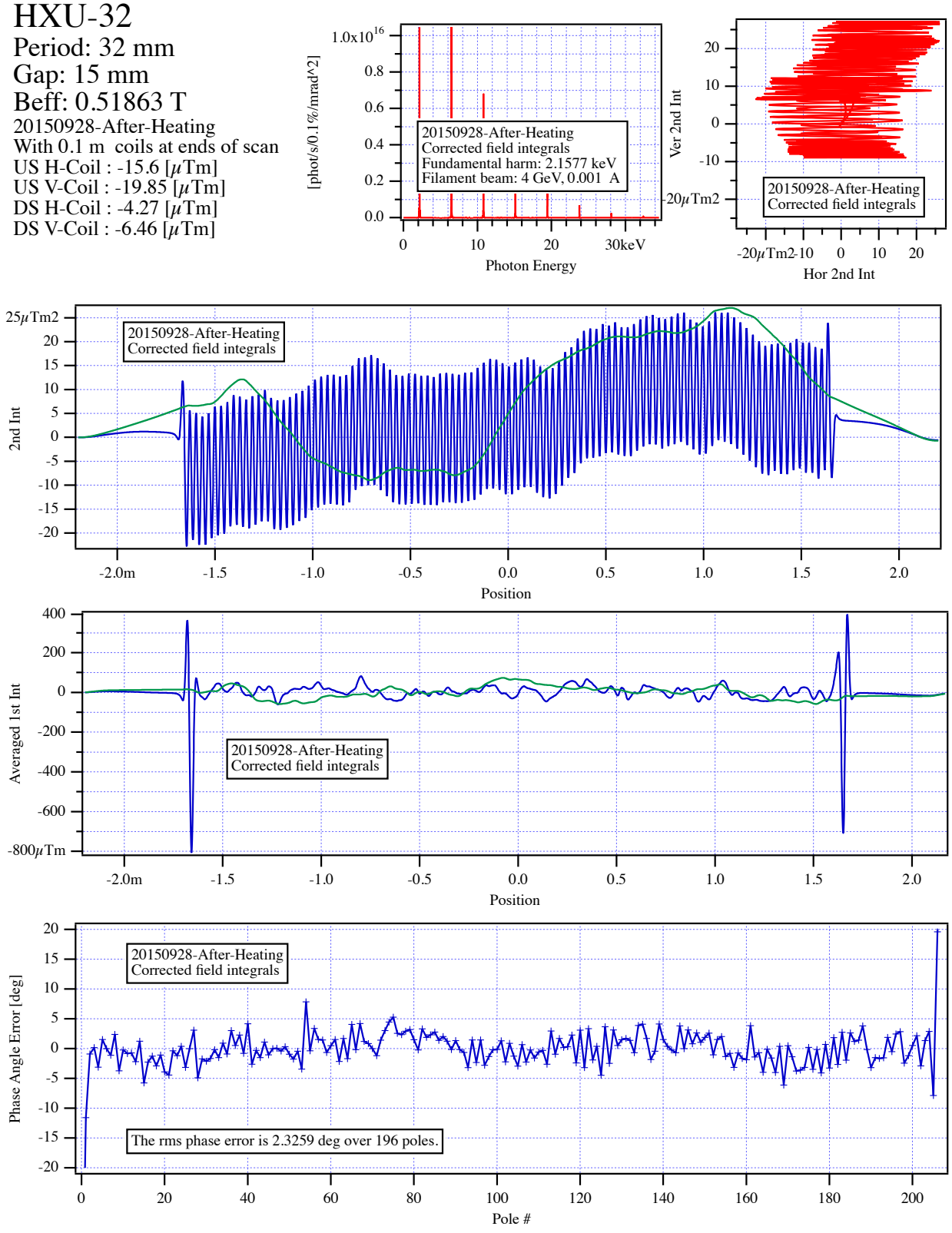

Figure 12: The measured fields, angles, trajectories and phase errors for the HXU-32 at 15 mm gap with the beam path corrected by virtual coils.

HXU-32
Period: 32 mm
Gap: 20 mm
Beff: 0.30968 T
20150928-After-Heating
Without correction coils
1st Int Ix : -13.39 [μTm]
1st Int Iy : -25.05 [μTm]
2nd Int Jx : -7.23 [μTm^2]
2nd Int Jy : -21.52 [μTm^2]
Beam energy: 4 GeV

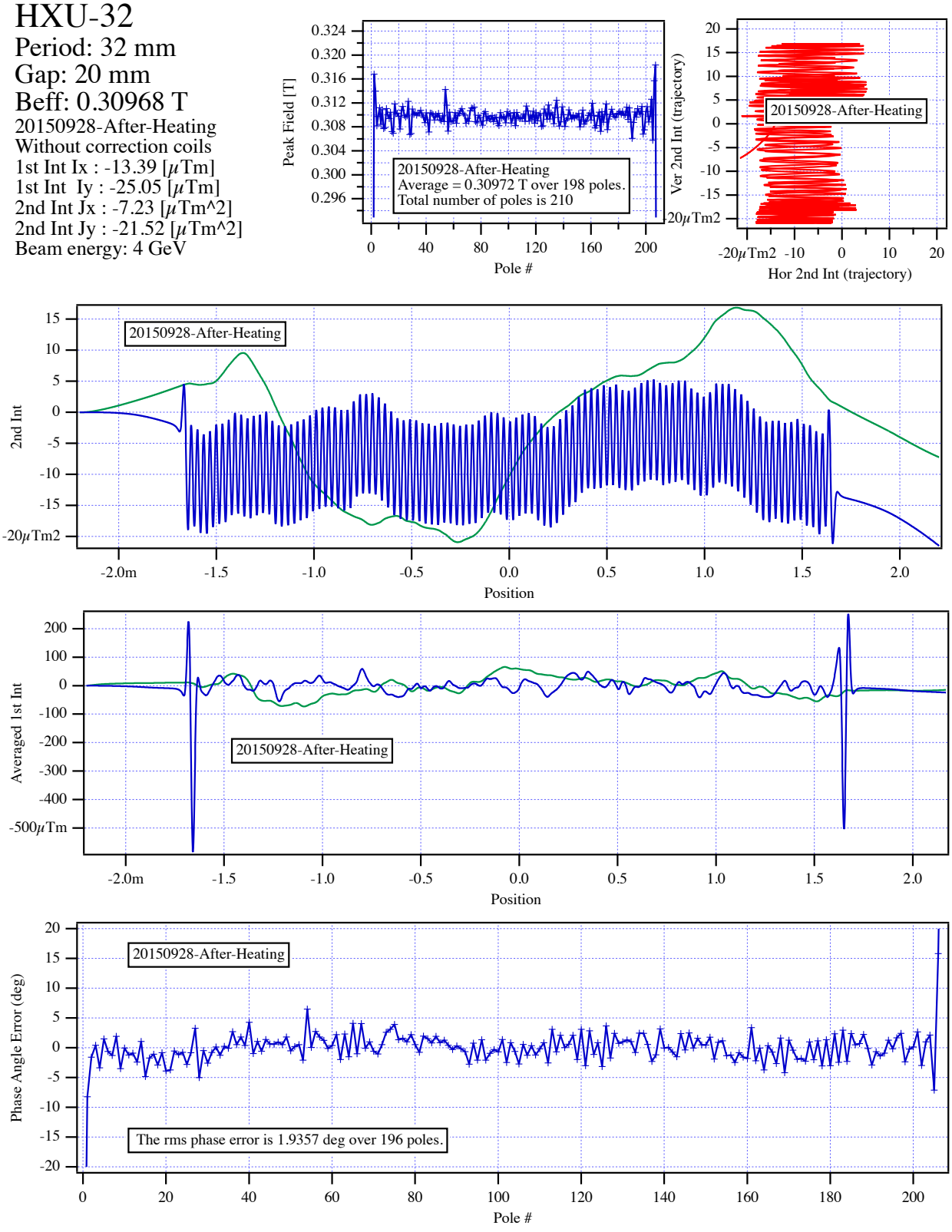

Figure 13: The measured fields, angles, trajectories and phase errors for the HXU-32 at 20 mm gap.

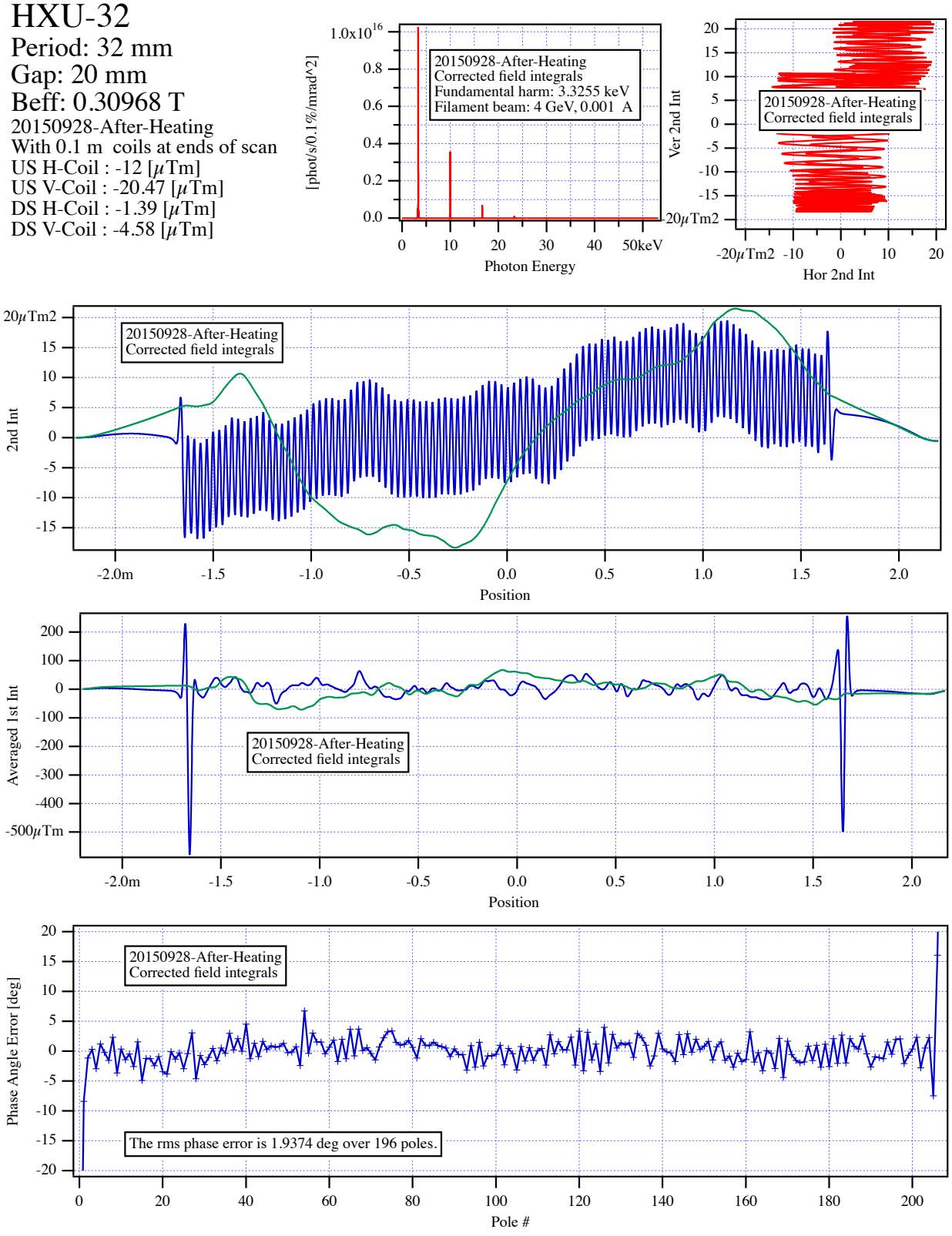

Figure 14: The measured fields, angles, trajectories and phase errors for the HXU-32 at 20 mm gap with the beam path corrected by virtual coils.

HXU-32
Period: 32 mm
Gap: 25 mm
Beff: 0.18755 T
20150928-After-Heating
Without correction coils
1st Int Ix : -2.65 [μTm]
1st Int Iy : -27.44 [μTm]
2nd Int Jx : 21.11 [μTm^2]
2nd Int Jy : -18.06 [μTm^2]
Beam energy: 4 GeV

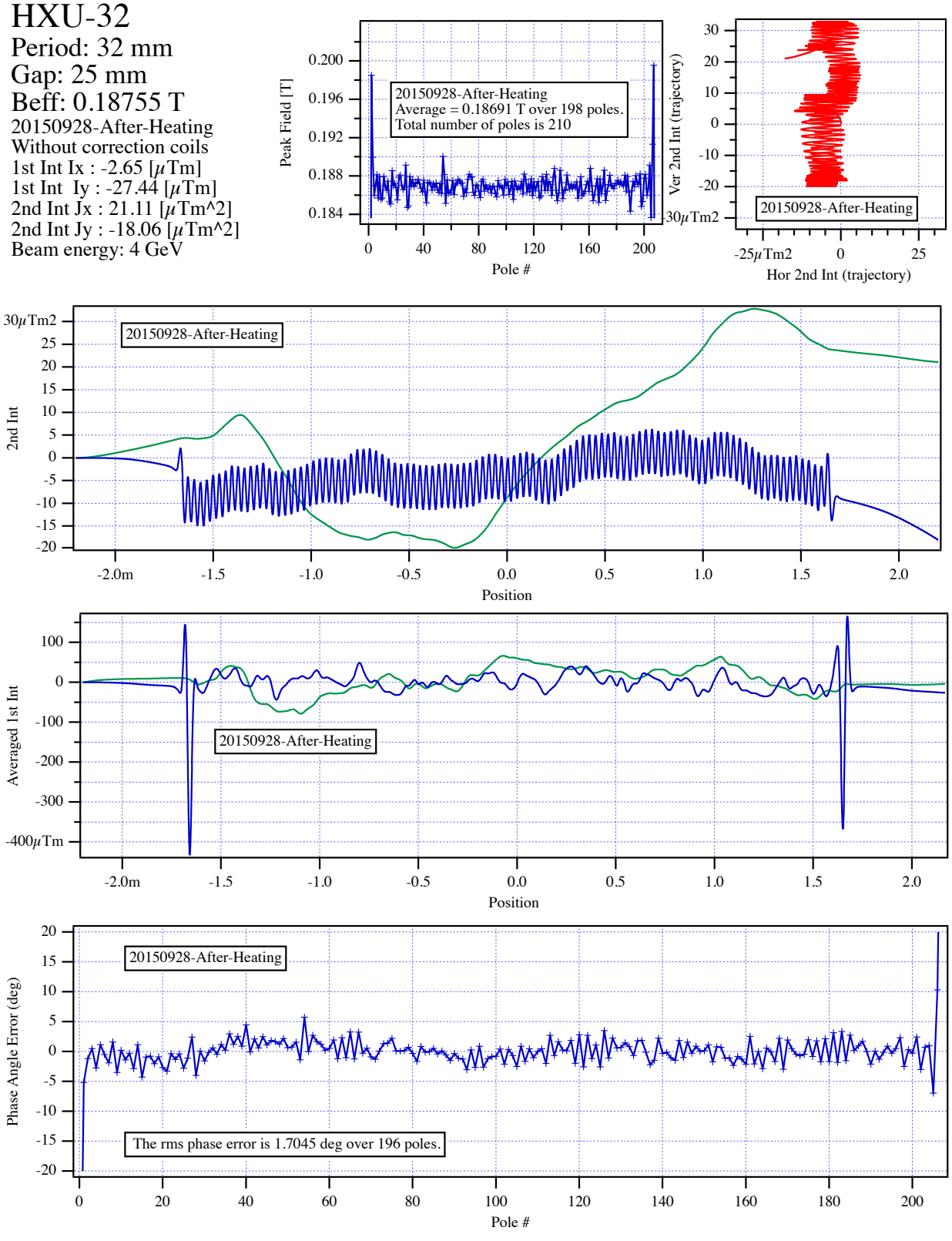

Figure 15: The measured fields, angles, trajectories and phase errors for the HXU-32 at 25 mm gap.

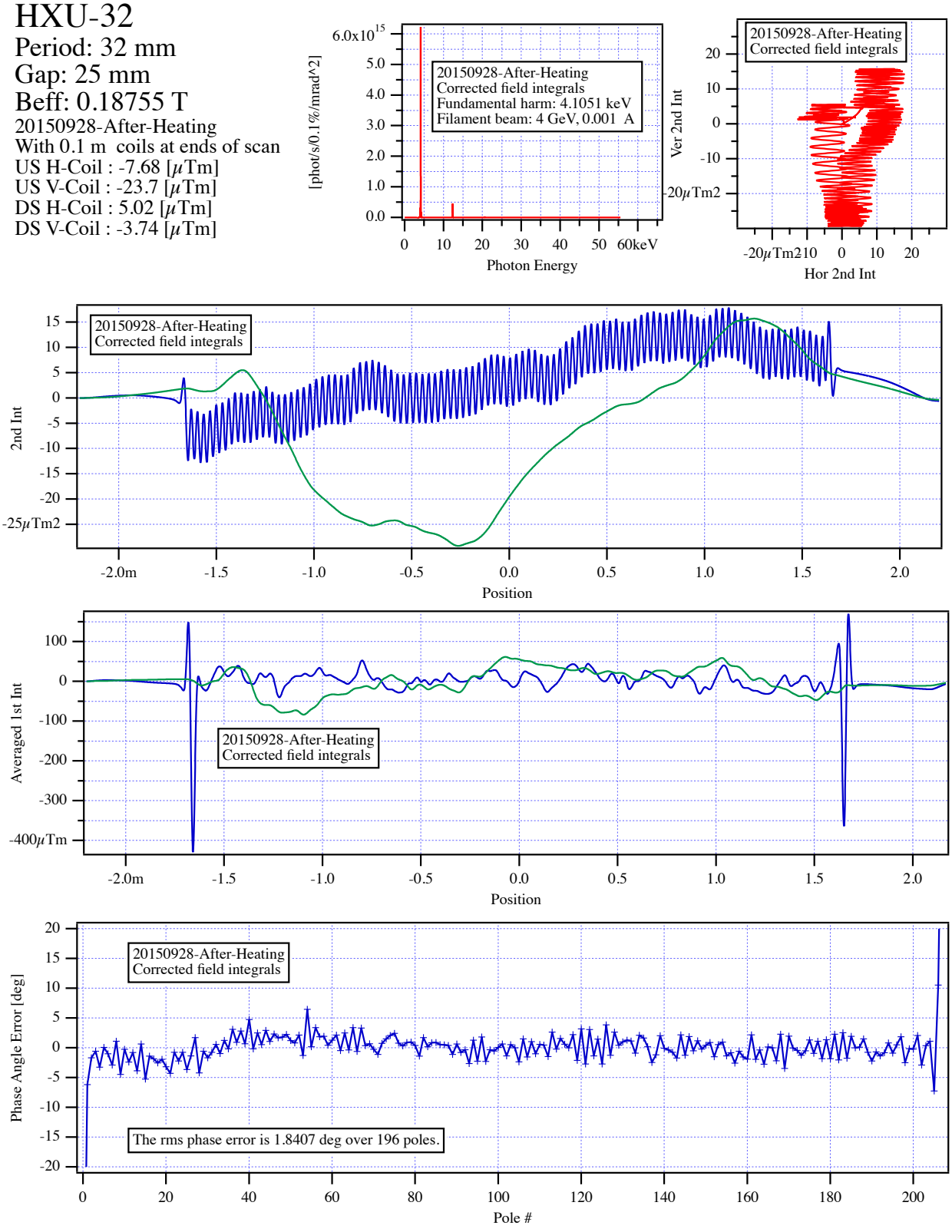

Figure 16: The measured fields, angles, trajectories and phase errors for the HXU-32 at 25 mm gap with the beam path corrected by virtual coils.

4.7 Gap 50, 100 and 180 mm

The measured vertical fields for the gaps 50, 100 and 180 mm are shown in Figure 17 and the corresponding horizontal fields are shown in Figure 18 .

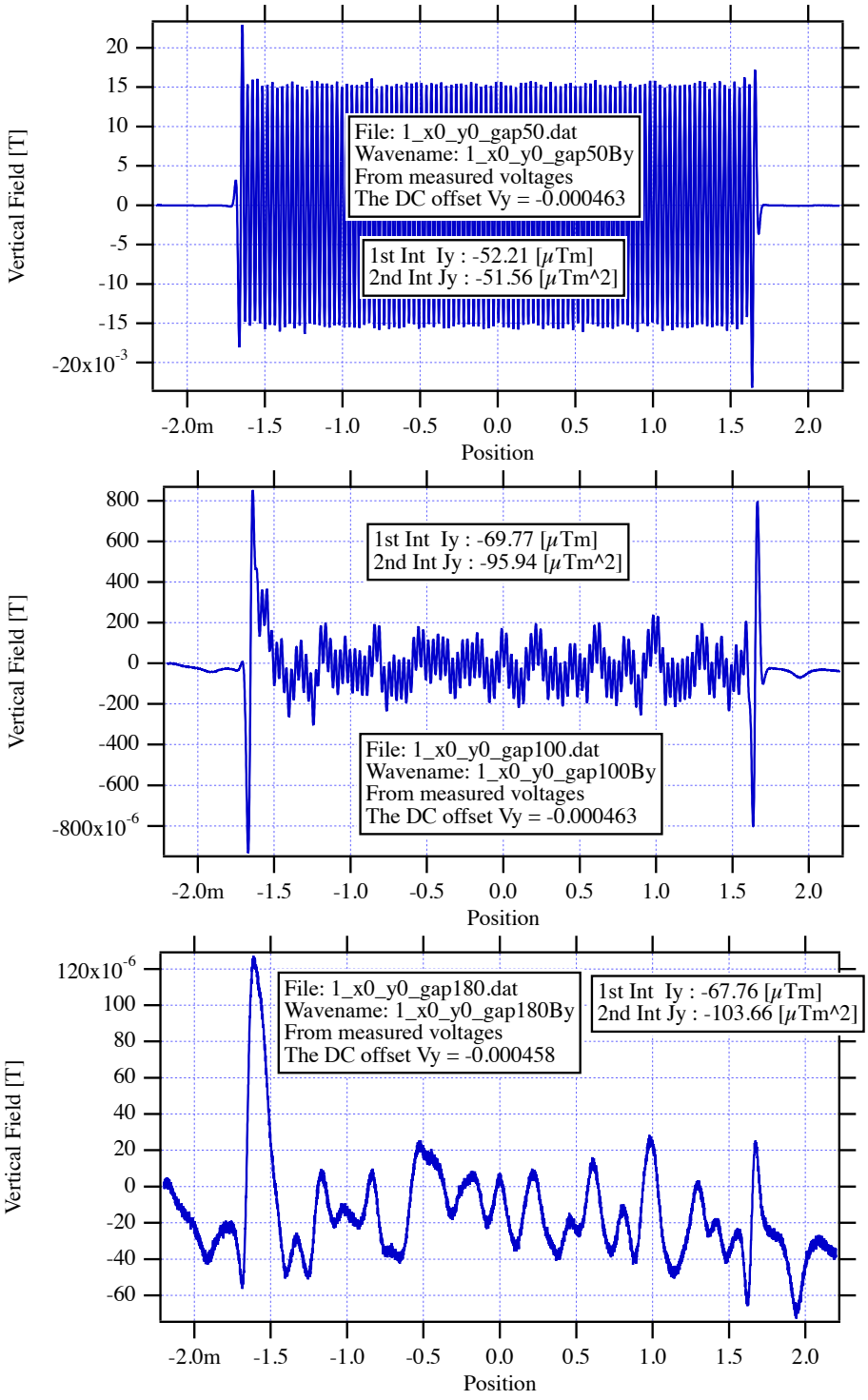

Figure 17: The measured vertical fields for the HXU-32 at the gaps 50, 100 and 180 mm.

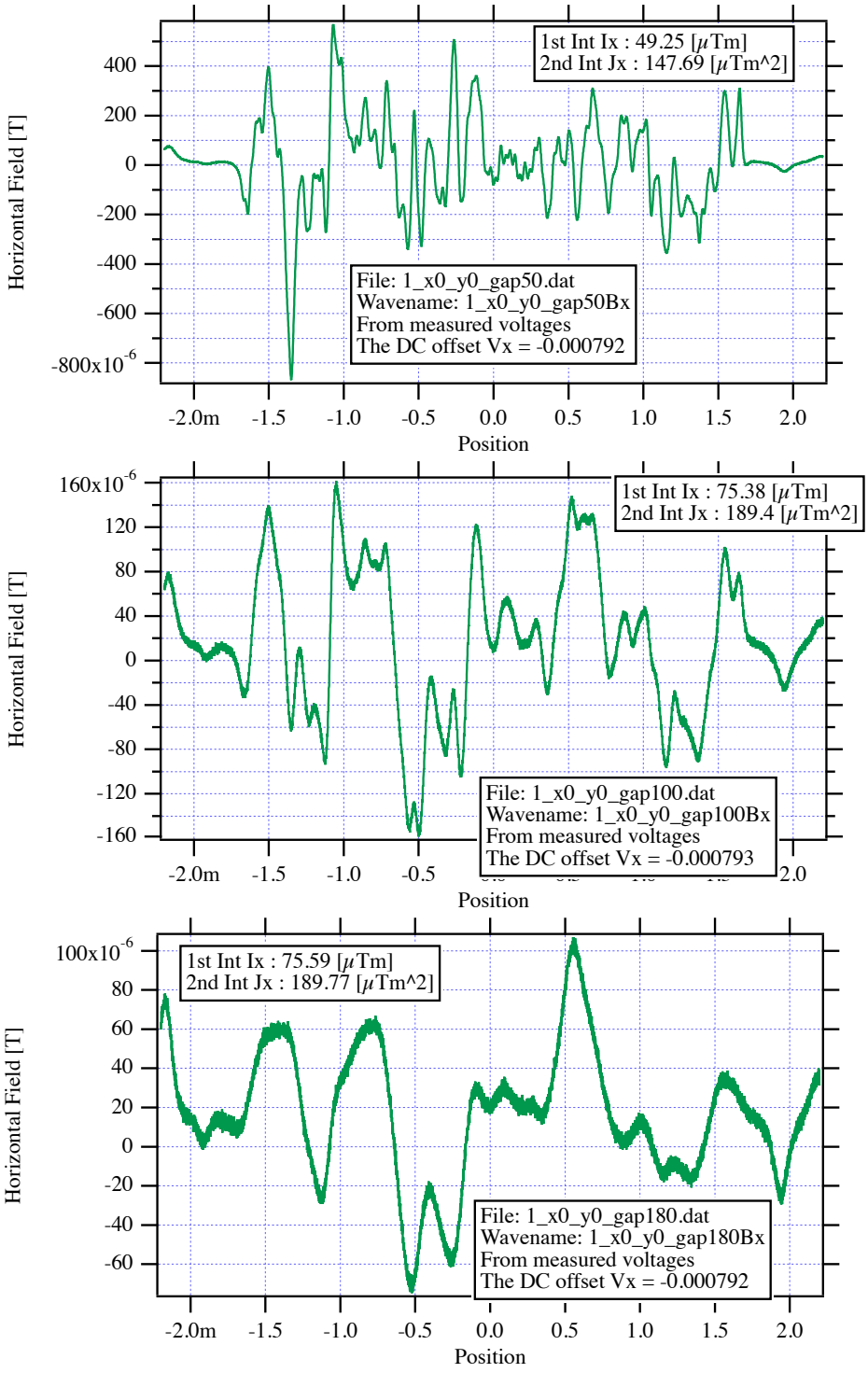

Figure 18: The measured horizontal fields for the HXU-32 at the gaps 50, 100 and 180 mm.

5 Repeatability of the effective field

The repeatability of the effective field has been measured by making 10 cycles over 8 gaps, giving in 80 measurements. The 8 gaps in the cycle ar 7.2, 8, 10, 15, 20, 15, 10, and 8 mm. The effective field has here, in the case of the repeatibilty measurements, been calculated using a fourier analysis of the measured magnetic fields.

Figure 19 shows the gaps during the repeatbility measurements. Figure 20 shows the measured effective field duing the repeatbility measurements. Figure 21 shows the measured deviation of the effective field duing the repeatbility measurements. Figure 22 shows the measured deviation of the effective field duing the repeatbility measurements as a function of the gap.

Table 3 shows data from the repeatability measurements.

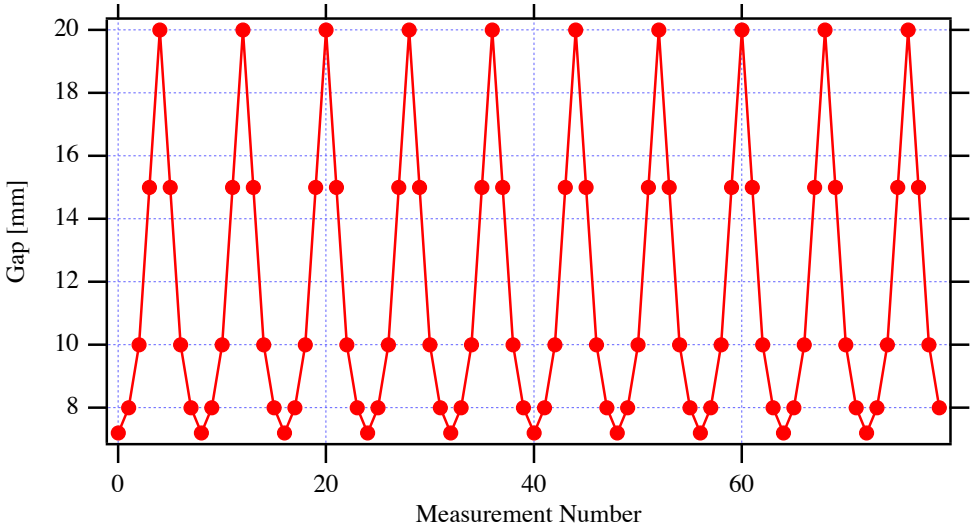

Figure 19: The gaps at the reapatability measurements of the effective field.

Table 3: Data from Beff repeatability measurements

Gap mm	Aver Beff T	RMS Dev G	RMS Dev $\times 10^{-4}$	Max ΔBeff/Beff $\times 10^{-4}$	Min ΔBeff/Beff $\times 10^{-4}$
7.2	1.2828	1.2963	1.0105	2.4176	-0.96694
8	1.1590	0.9308	0.80312	1.755	-1.7545
10	0.90402	0.55121	0.60973	1.4864	-0.91162
15	0.51756	0.25639	0.49538	0.79579	-0.95356
20	0.30887	0.11735	0.37995	0.4836	-0.51988

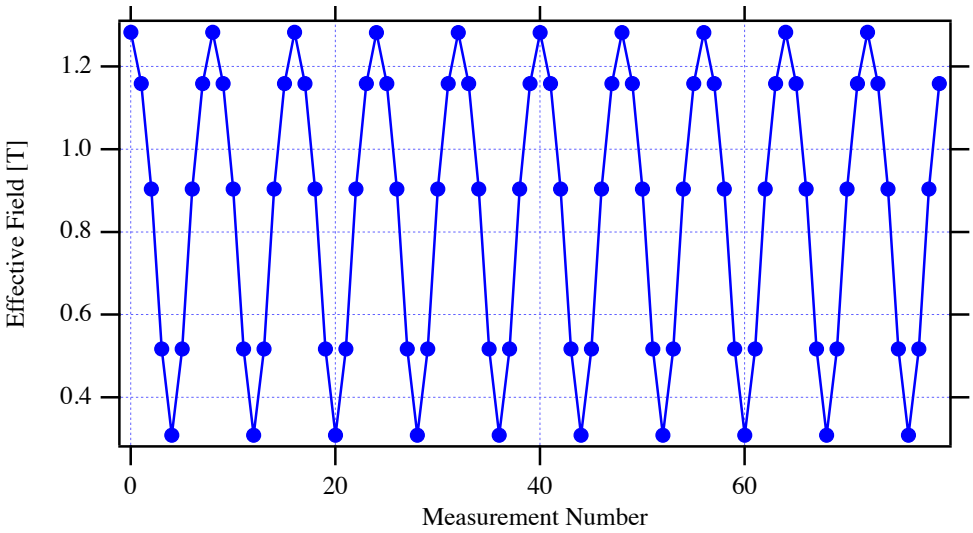

Figure 20: The measured effective field at the reapatability measurements.

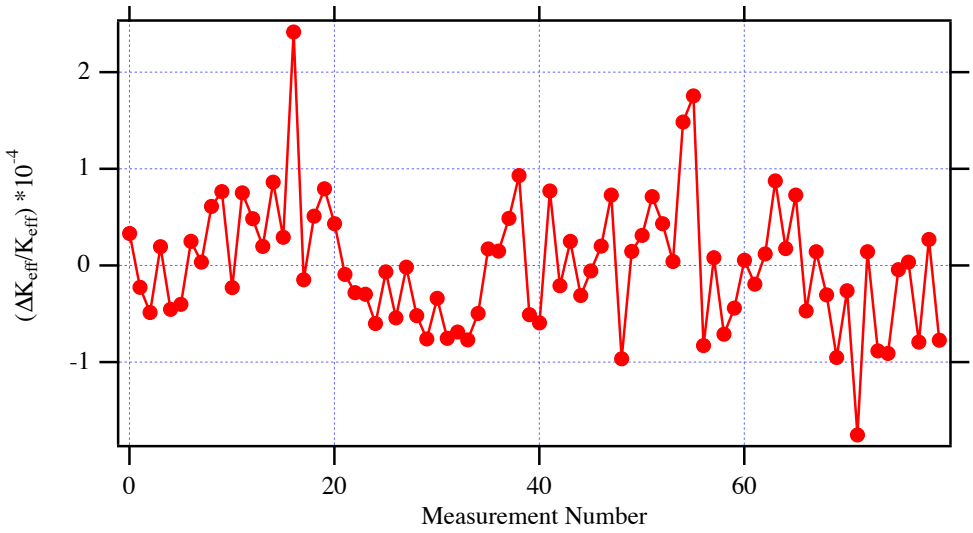

Figure 21: The measured deviation of the effective field at the reapatability measurements.

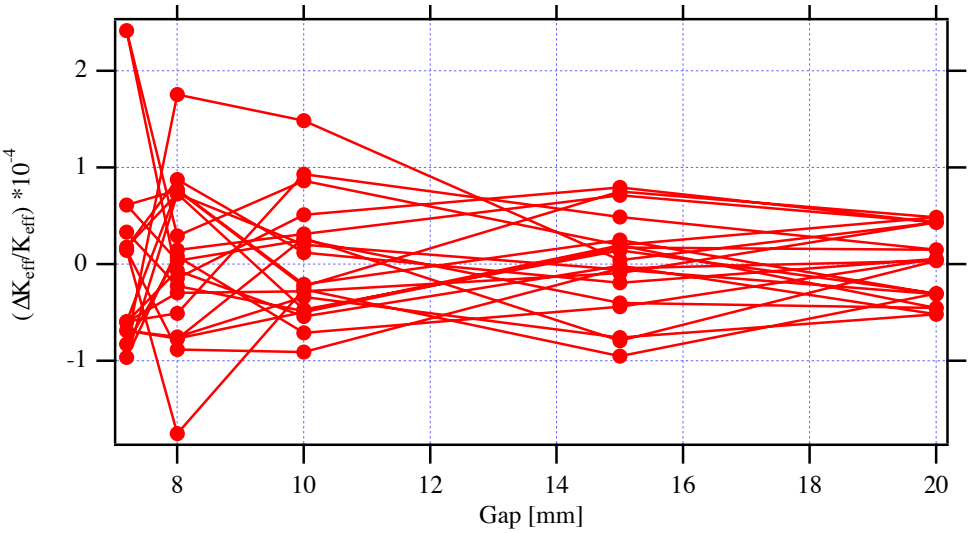

Figure 22: The measured deviation of the effective field at the reapatability measurements as a function of the gap.